catalysts

MDPI

Article

Synthesis of Nanostructured TiO_2 Microparticles with High Surface Area

Lev Matoh *, Boštjan Žener, Tina Skalar and Urška Lavrenčič Štangar

Faculty of Chemistry and Chemical Technology, University of Ljubljana, Večna Pot 113, SI-1000 Ljubljana, Slovenia; bostjan.zener@fkkt.uni-lj.si (B.Ž.); Tina.Skalar@fkkt.uni-lj.si (T.S.); urska.lavrencic.stangar@fkkt.uni-lj.si (U.L.Š.)

* Correspondence: lev.matoh@fkkt.uni-lj.si

Abstract: Hydrothermal reactions represent a simple and efficient method for the preparation of nanostructured TiO_2 particles that could be of interest as photocatalysts or catalytic supports. Although the particle size is in the range of 2–5 μm, the nanostructures composing the particles ensure a large specific surface area with values above 100 m^2/g. The effects of the different synthesis parameters on the morphology, photocatalytic activity, and stability of the prepared material were studied. The surface morphology of the prepared TiO_2 powders was studied by scanning electron microscopy (SEM). To further characterize the samples, the specific surface area for different morphologies was measured and the photocatalytic activity of the prepared powders was tested by degrading model pollutants under UV irradiation. The results show that the initial morphology had little effect on the photocatalytic properties. On the other hand, the final calcination temperature significantly increased the degradation rates, making it comparable to that of P25 TiO_2 (particle size 20–30 nm).

Keywords: TiO_2; high surface area; photocatalysis; nanostructured particles

Citation: Matoh, L.; Žener, B.; Skalar, T.; Štangar, U.L. Synthesis of Nanostructured TiO_2 Microparticles with High Surface Area. *Catalysts* **2021**, *11*, 1512. https://doi.org/10.3390/catal11121512

Academic Editor: Abel Santos

Received: 17 November 2021
Accepted: 9 December 2021
Published: 11 December 2021

1. Introduction

Although TiO_2 photocatalysis for water treatment has been extensively researched in recent decades [1–9], its use in practice is still limited. This is partially due to the lack of efficient reactor systems that can treat large volumes of water economically and in a timely manner [1,10,11].

An important parameter for photocatalysts is their specific surface area. To increase it, the particle size is usually reduced, with the most active TiO_2 photocatalysts having particle sizes in the range of 10 to 30 nm. When used as a photocatalyst, the best results are obtained when the particles are suspended in a solution. However, an additional step is then required to separate the particles from the solution after the reaction. Since filtration of nanoparticles is difficult and expensive, larger particles with a morphology that promotes a high specific surface area are desirable. This would theoretically allow the construction of a flow through slurry reactor that could combine the efficiency of suspended particles with the ease of use of an immobilized photocatalyst [12–17].

Hydrothermal reactions represent a simple and efficient method for the preparation of nanostructured TiO_2 particles that could be of interest as photocatalysts or catalyst supports. Although there are many papers on the hydrothermal synthesis of TiO_2, few of them investigate the effects of a strongly alkaline solution on the morphology of the prepared materials. Some research papers addressed the modification of the surface of already prepared TiO_2 particles, where they successfully prepared nanotubes and nanoparticles as powders or deposited them on various supports. Preparation of larger particles has also been explored from already prepared TiO_2 or metallic titanium [18–22]. However, to our knowledge, the effect of synthesis parameters and calcination temperature on the

morphology and photocatalytic activity of TiO_2 materials prepared from fully dissolved Ti ions in an alkaline solution by hydrothermal methods has not been fully explored.

In this work, we present a simple method to prepare nanostructured TiO_2 particles. Although the particle size is in the range of 2–5 μm, the nanostructures composing the particles ensure a large specific surface area with values above 100 m^2/g. The powders were prepared by a hydrothermal method in a strongly alkaline solution. The nanomorphology of the larger particles can be easily controlled by adjusting the reaction parameters. By optimizing key parameters, we were able to increase the yield of the reaction compared to previously reported results. The morphology of the prepared samples is stable and does not change even after calcination at up to 500 °C. The short reaction times, scalability, and high titanium concentrations in the reaction solution also allow the production of larger quantities of the powders.

2. Results

2.1. Optimizing Synthesis

Although methods to prepare flower-like TiO_2 particles by a hydrothermal process in an alkaline solution have been described previously, they were complicated and had low yields while often requiring days of mixing [21]. By optimizing the preparation of the starting solution, we were able to increase the amount of titanium dissolved while reducing the time required to prepare the precursor solution to less than 30 min.

The goal in preparing the initial solution was to obtain the maximum concentration of titanium ions that could still be completely dissolved. The actual mechanism of dissolution is still unknown, but from the experiments, it appeared that the addition of H_2O_2 at the beginning was crucial. However, the addition of more H_2O_2 to the initial solution had no effect on the morphology or photocatalytic activity though.

The use of titanium alkoxides as precursors is also possible. It does not affect the final result, but it significantly increases the time required to prepare the starting solution.

The yield of the reaction was between 80% and 90% after washing and calcination. The scale up of the synthesis was tested by increasing the volume of the starting solution to 250 mL in a 300 mL autoclave, with no difference observed in the samples prepared. This suggests that larger quantities can be readily prepared.

A possible pathway for the formation of TiO_2 is shown in Figure 1. First, sodium metatitanate (Na_2TiO_3) was obtained from the hydrothermal reaction. Washing with 0.1 M HCl replaced the sodium ions with hydrogen, giving metatitanic acid (H_2TiO_3). During the final calcination, metatitanic acid decomposed to TiO_2 and H_2O.

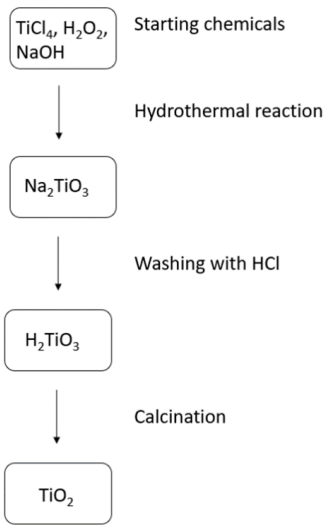

Figure 1. Scheme of TiO_2 formation.

2.1.1. Effect of Preparation Conditions on Morphology and Photocatalytic Activity of TiO_2 Particles

The morphology depends mainly on the parameters of the hydrothermal reaction. It is also important that all of the titanium precursor is dissolved in the solution before the reaction, otherwise completely different morphologies are formed. The size of the particles is 2–5 µm for the larger ones and about 0.5–1 µm for the smaller ones (Figure 2A) and is not significantly affected by changing the parameters, which allows the optimization of other properties while maintaining the ability to easily filter the particles after use.

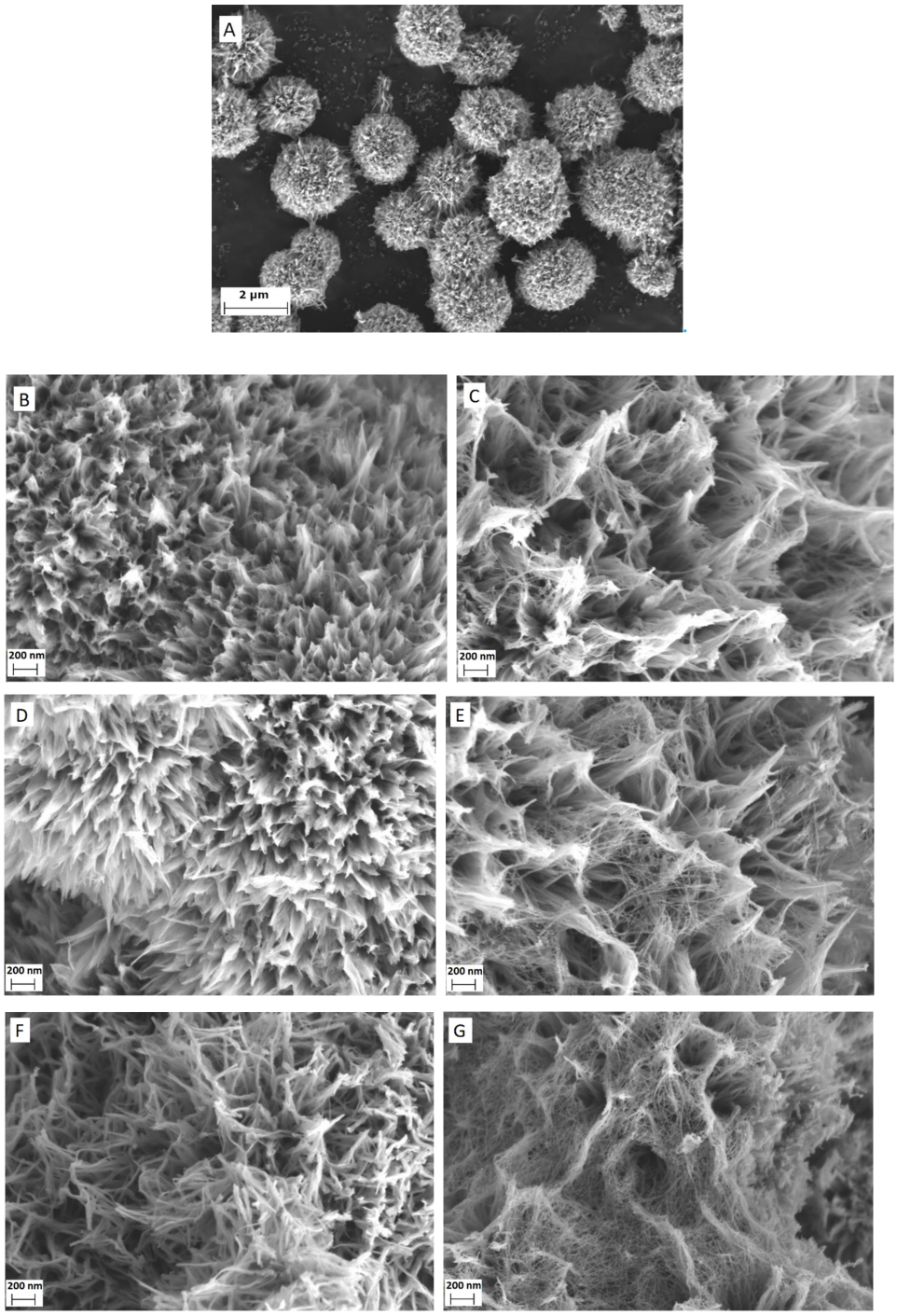

Figure 2. SEM images of samples prepared with different parameters of hydrothermal synthesis and calcinated at 500 °C. The designations (**A**–**G**) on the images correspond to sample names in Section 3.1.

Figure 2 shows SEM images of different samples (Supplementary Materials). From the results, it is evident that increasing the time or temperature of hydrothermal synthesis is interchangeable, while the amount of NaOH has a much more profound effect on the morphology. At low concentrations of NaOH, the particles consist of thicker fibres. When the concentration is increased to about 20 wt.%, the fibres are replaced by leaf-like structures, originating from the centre of the hemispherical particles. Further increase to 30 wt.%, retains the leaf-like structure, but the surface is covered with a thick mesh of very thin (−6 nm) fibres, resembling a spider web. This structure appears only on the surface of the particles and binds them together into larger clusters (Figure 2G).

The same thin mesh also appears at longer reaction times or higher temperatures. It can be assumed that the large particles are formed first during the reaction, but that these are partially dissolved during the course of the reaction, and the resulting material is deposited on the surface in the form of the thin fibres. This is confirmed when comparing the particles prepared at shorter times/lower temperatures, where the leaf-like structure is more densely packed compared to the others.

The thin mesh on the surface greatly increases the surface area of the material (Table 1) and the amount of adsorbed compounds on the surface. However, it does not increase the photocatalytic activity. This is probably due to the diameter of the fibres being too small, which results in an increased recombination rate, as the charge carriers cannot be separated efficiently [23].

Table 1. Specific surface area values for the prepared samples. The sample designations are the same as in Section 3.1.

Sample	Surface Area [m^2/g]
A	133 ± 0.7
B	135 ± 0.9
C	140 ± 0.9
D	121 ± 0.7
E	147 ± 0.8
F	114 ± 0.8
G	160 ± 1.4

Table 1 shows the results of the specific surface area measurements, which are in good agreement with the morphologies seen on the SEM images. Longer reaction times and higher reaction temperatures increase the surface area. The same effect is observed when the amount of NaOH is increased.

Due to the high specific surface area of the prepared samples, the adsorption of the pollutant on the surface has a great influence on the photocatalytic reaction. Therefore, the photocatalytic activity was tested in two steps by separating the adsorption and degradation reactions. All samples were first stirred in the dark to saturate the surface of the photocatalyst. Then, the suspension was exposed to UV illumination. Interestingly, adsorption was faster than photocatalytic degradation, which is why the reaction appears to be 0-order after the light is turned on, rather than 1st-order, as would be typical for photocatalysis.

Figure 3 shows the results of the photocatalytic experiments for different samples treated at 500 °C. For the first 35 min, the samples were stirred in the dark to determine the effect of adsorption on the concentration of the dye. After 35 min, the UV lights were turned on and photocatalytic degradation began. During the first 10 min of illumination, a steeper drop in concentration is observed, which is due to the presence of oxygen in the initial solution. After the oxygen is used up, a linear decrease in dye concentration follows.

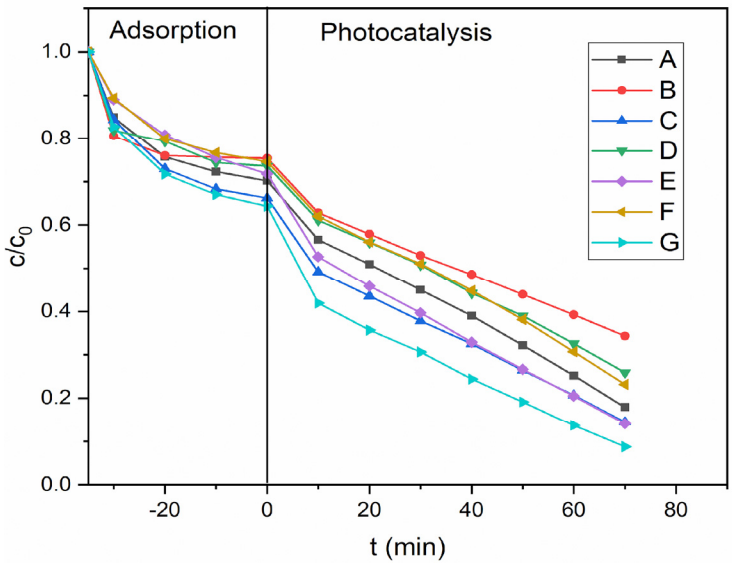

Figure 3. Adsorption and photocatalytic degradation of PB with different prepared samples ($\gamma(TiO_2)$ = 0.25 g/L).

It can be seen that the photocatalytic activity is comparable between the samples calcinated at the same temperature, as the slope of the curves in the linear part is very similar (Table 2), although the initial morphologies and surface areas are quite different. However, there is a clear difference in the amount of dye adsorbed, which correlates to some extent with the different surface areas of the samples.

Table 2. Reaction constants from the linear part of photocatalytic degradation ($\gamma(TiO_2)$ = 0.25 g/L).

Sample	k [μg L^{-1} min^{-1}]
A	76 ± 5
B	75 ± 2
C	71 ± 2
D	75 ± 3
E	76 ± 6
F	82 ± 2
G	69 ± 2

It is also worth noting that the concentration of the photocatalyst ($\gamma(TiO_2)$ = 0.25 g/L) is lower than usual, to obtain better measurements and to limit the adsorption on the surface. When the amount is increased to 1 g/L, most of the dye is adsorbed on the surface and the photocatalyst changes its color from white to gray. After 15 min of UV illumination, the samples return to their original color, as the adsorbed dye is degraded.

2.1.2. Effect of Thermal Treatment on Morphology and Photocatalytic Activity of TiO_2 Particles

To optimize the photocatalytic activity of the material, different calcination temperatures were tested and the effects on activity and morphology were determined. Figure 4 shows the results of XRD measurements for different treatment temperatures. At higher temperatures, the diffraction peaks become more intense and defined, indicating a higher degree of crystallinity in the samples. This in turn also affects the photocatalytic activity. All peaks visible on the diffraction patterns correspond to the anatase modification of TiO_2.

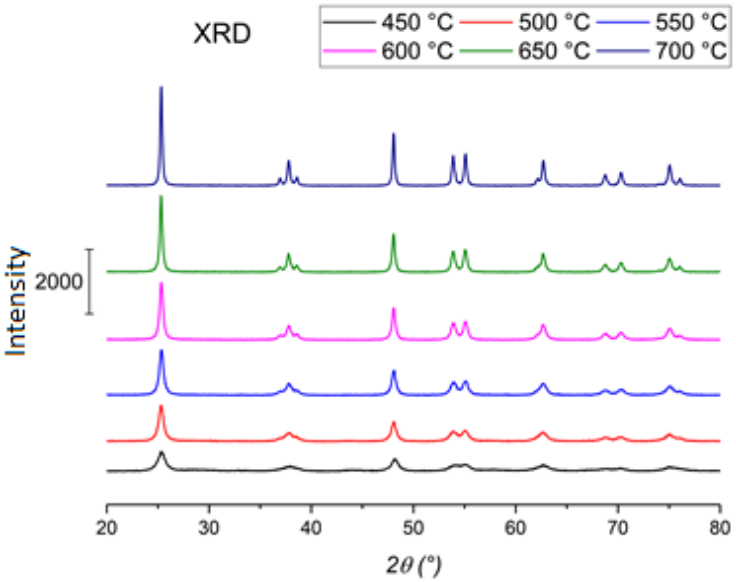

Figure 4. X-ray diffraction (XRD) patterns of samples treated at different temperatures.

The morphology of the material remains unchanged up to 500 °C, after which some "melting" of the surface can be seen (Figure 5). Even though the specific surface area of the samples decreases with increasing calcination temperature (Table 3), the increase in photocatalytic activity is greater due to the higher crystallinity. The XRD measurements were also used to calculate the average size of nanocrystallites for the material treated at different temperatures (Table 3). As expected, higher temperatures increase the size of the crystallites.

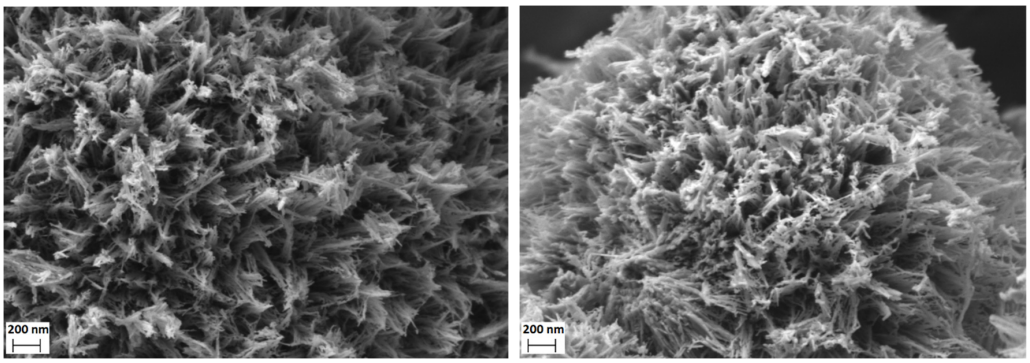

Figure 5. SEM images of samples (synthesis A) treated at 650 °C (**left**) and 700 °C (**right**).

Table 3. Specific surface areas and size of anatase crystallites of sample A, calcinated at different temperatures.

Sample	Surface Area [m^2/g]	Crystalite Diameters [nm]
A-450	185 ± 1.2	10
A-500	133 ± 0.7	14
A-550	113 ± 0.8	18
A-600	93 ± 0.7	23
A-650	55 ± 0.3	31
A-700	39 ± 0.2	44

Unlike the parameters of the hydrothermal synthesis, the temperature of the final thermal treatment has a great influence on the photocatalytic activity of the prepared material. Figure 6 shows the results of photocatalytic activity testing for sample A treated at different temperatures, starting from the end of the adsorption phase. The activity of the

samples increases up to 650 °C (Table 4), which correlates with the increased crystallinity of the samples treated at higher temperatures.

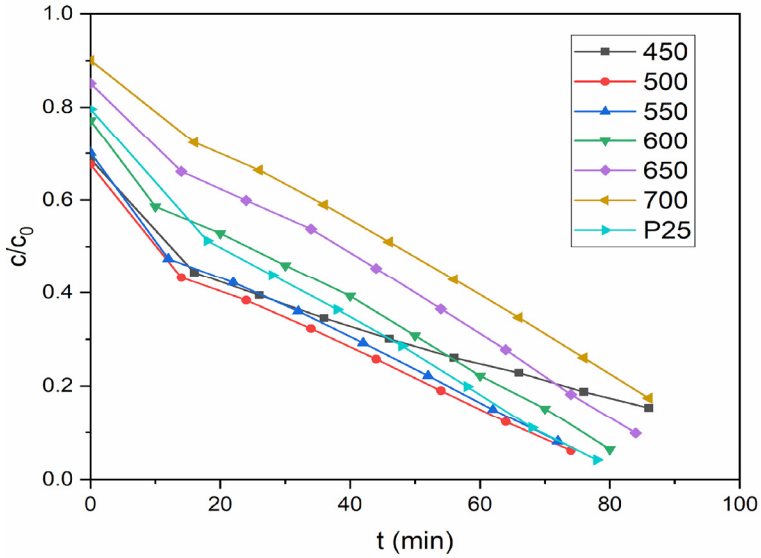

Figure 6. Photocatalytic degradation of PB with sample A calcined at different temperatures ($\gamma(TiO_2)$ = 0.25 g/L).

Table 4. Reaction constants from the linear part of photocatalytic degradation for samples calcinated at different temperatures ($\gamma(TiO_2)$ = 0.25 g/L).

Sample	k [μg L^{-1} min^{-1}]
P25	96 ± 5
A-450	49 ± 5
A-500	76 ± 5
A-550	80 ± 9
A-600	90 ± 7
A-650	99 ± 4
A-700	95 ± 7

Comparison of the slopes of the linear part for samples treated at 500 °C (k = 76 μg L^{-1} min^{-1}) and the samples treated at 650 °C (k = 99 μg L^{-1} min^{-1}) shows an increase of about 30% in photocatalytic activity. The amount of dye adsorbed on the surface decreases at higher treatment temperatures, which correlates with the lower surface area of the samples. To compare the prepared materials with other TiO_2 photocatalysts, the same photocatalytic activity tests were also performed with Aeroxide TiO_2 P25 from Evonik, which showed comparable activity to the samples treated at 650 °C or higher.

2.2. Investigation of Catalyst Stability

The reusability of the photocatalyst was tested for sample A. The results for the linear part of the photocatalytic degradation are presented in Figure 7. The amount of dye adsorbed on the surface decreases with each use, which could be due to insufficient removal of the dye between experiments. However, the degradation rate constants remain unchanged, with values ranging from 75 to 80 μg L^{-1} min^{-1}, from which it can be concluded that the photocatalytic activity of the sample does not decrease with repeated use.

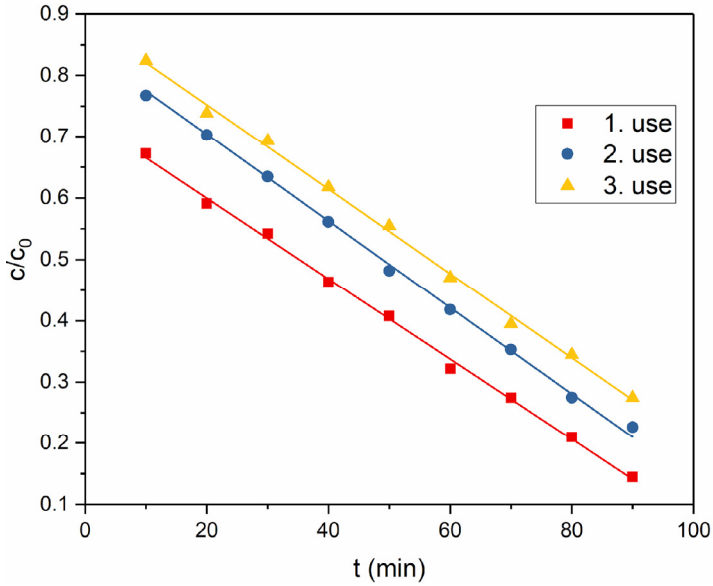

Figure 7. Reusability experiments with sample A (γ (TiO_2) = 0.25 g/L).

SEM image of sample A after repeated use is shown in Figure 8. While there is some damage to the particles, it is minor and likely the result of drying and scraping the sample after each use rather than the photocatalytic experiments themselves.

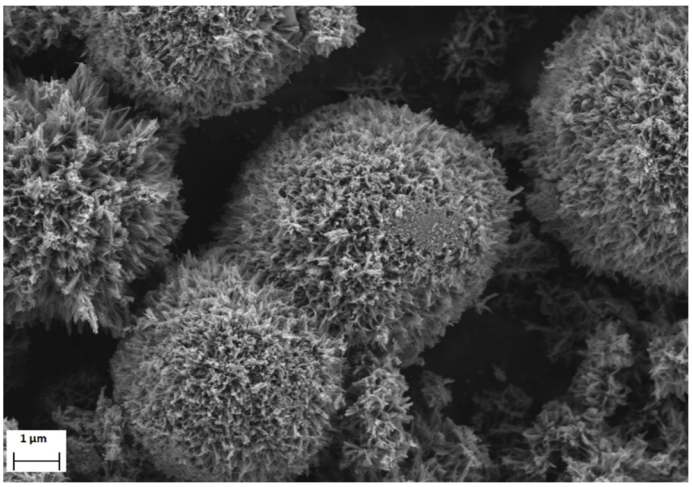

Figure 8. SEM images of sample A after 3 photocatalytic experiments.

2.3. Investigation of the Degradation of Ibuprofen and Diclofenac Using the Prepared TiO_2

Since pharmaceuticals are also a critical problem in wastewater, we also tested the degradation of ibuprofen and diclofenac using sample A calcined at 500 °C. Figure 9 shows the results of the experiments. It can be seen that adsorption is minimal in these two cases, unlike the tests with the dye. This is due to the absence of electrostatic interactions which are present between plasmocorinth B (negative charge) and TiO_2 (positively charged surface at pH 4). The degradation itself is also faster compared to the dye and is completed in ~20 min for diclofenac and ~40 min for ibuprofen.

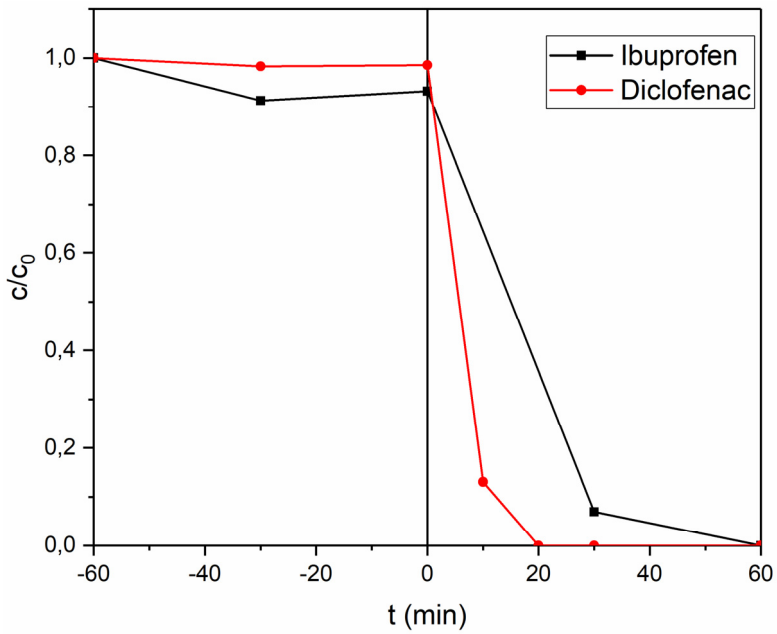

Figure 9. Adsorption and photocatalytic degradation of ibuprofen and diclofenac using sample A ($\gamma(TiO_2)$ = 0.5 g/L).

3. Materials and Methods

3.1. Synthesis

To determine and evaluate the effect of the synthesis parameters on the morphology and photocatalytic activity of the prepared powders, several samples were synthesized by modifying the basic synthesis as follows: 0.6 mL of H_2O_2 (30% solution) was added to 30 mL of dH_2O, then 0.24 mL of $TiCl_4$ was added dropwise while stirring to obtain a red solution; then 7.5 g of NaOH was added stepwise (~20 wt.%), after which we obtained a clear colorless solution. The addition of NaOH facilitates the dissolution of titanium ions. The solution was transferred to a Teflon-lined autoclave and heated at 150 °C for 3 h to precipitate the TiO_2 particles from the solution. After the reaction, the product was washed thoroughly with dH_2O and then with 0.1 M HCl to remove sodium ions from the product. After washing again with dH_2O, the product was dried at 100 °C and then calcinated in air at 500 °C for 30 min to promote crystallization of TiO_2.

By changing the amount of NaOH (10, 20, 30%w), the temperature (120, 150, 180 °C) and the time (1.5, 3, 4.5 h) of the hydrothermal reaction, it is possible to strongly influence the morphology of the prepared material. However, this did not affect their photocatalytic properties. On the other hand, increasing the calcination temperature had a great influence on the photocatalytic properties of the prepared samples. The specific synthesis parameters for each sample are listed in Table 5.

Table 5. Specific synthesis parameters of different prepared samples (time and temperature of hydrothermal reaction, NaOH content).

Sample	Parameters
A	t = 3 h; T = 150 °C; w(NaOH) = 20%
B	t = 1.5 h; T = 150 °C; w(NaOH) = 20%
C	t = 4.5 h; T = 150 °C; w(NaOH) = 20%
D	t = 3 h; T = 120 °C; w(NaOH) = 20%
E	t = 3 h; T = 180 °C; w(NaOH) = 20%
F	t = 3 h; T = 150 °C; w(NaOH) = 10%
G	t = 3 h; T = 150 °C; w(NaOH) = 30%

3.2. Characterization

The XRD pattern of the powder was acquired using a PANalytical X'Pert PRO MPD instrument in the 2θ range of 20–80° with a step size of 0.034°. The average diameter of crystallites, coherently diffracting crystalline domains, was calculated using the *Scherrer equation*.

The morphology and size of the particles of the prepared samples were examined using a scanning electron microscope (SEM, Ultra Plus Zeiss) at 2 kV.

The Brunauer–Emmett–Teller (BET) specific surface area analyses were performed using the 'ASAP 2020 Micromeritics' instrument. Samples were pre-prepared using degas procedure with setpoint vacuum (50 mmHg), heated up to 300 °C and held at final conditions for one hour. Samples were analyzed under nitrogen atmosphere (adsorption-desorption isotherms at 77 K) in a volumetric working device. Specific surface areas were calculated using ten point values for relative pressures between 0.01 and 0.3.

3.3. Photocatalytic Tests

Photocatalytic activity was determined and compared by observing the degradation of plasmocorinth B in deionized water (initial concentration: γ = 12 mg/L; pH = 4). The concentration of the photocatalyst was 0.25 g/L in all experiments. The suspension was continuously stirred and illuminated with two *UV Black Light Blue* (UV BLB) lamps and one *Actinic Blue* lamp (λ = 365 nm) with a total light intensity of 20 W/m^2. The activity was determined by measuring the absorption spectra of the dye at different time intervals.

UV–Vis absorption spectra were recorded using an Agilent Cary 60 UV–Vis spectrophotometer in the wavelength range λ = 400–800 nm. The absorbance value at 550 nm was used to plot the change in concentration of the dye. Prior to measurement, TiO_2 particles were removed from the suspension by filtration through a syringe filter with a pore size of 0.45 μm after the filter surface was saturated with the dye, to prevent additional removal during filtration. For reusability experiments the photocatalyst was removed by centrifugation and stored for the next experiment.

Reaction rate constants were calculated by multiplying the slope of the linear part of the graph by the initial mass concentration of the dye solution. The margin of error was calculated from at least 3 experiments.

Experiments with ibuprofen (γ = 10 mg/L) and diclofenac (γ = 4 mg/L) were performed in the same way, but the determination of concentration was done by using HPLC. The specific parameters were: mobile phase—50% acetonitrile, 50% 0.1% acetic acid; flow rate—0.7 mL/min; column—Poroshell C-18 (Agilent); injected volume: ibuprofen—5 μL; diclofenac—20 μL; UV detector: ibuprofen—222 nm; diclofenac—275 nm.

In order to separate the adsorption and degradation reactions, all tests were initially performed in the dark and illumination started once the maximum amount of dye or pharmaceutical was adsorbed on the surface.

4. Conclusions

The results of the study show that the parameters of hydrothermal synthesis strongly influence the morphology of the prepared samples, while calcination has a dominant effect on the photocatalytic activity of the samples. Reusability experiments show that the photocatalyst is stable and the photocatalytic activity does not decrease with repeated use. The prepared powders can efficiently degrade organic pollutants in photocatalytic reactions at rates comparable to nanoparticles of TiO_2, but their removal is much easier since classical filtration is possible. In combination with tangential flow filtration, a flow-through slurry reactor could potentially be developed.

Supplementary Materials: The following are available online at https://www.mdpi.com/article/10.3390/catal11121512/s1, Figure S1: EDS spectra of sample A (20 % NaOH), Figure S1: EDS spectra of sample F (10 % NaOH), Figure S2: EDS spectra of sample G (30 % NaOH), Figure S3: EDS spectra of uncalcined sample A.

Author Contributions: Conceptualization, L.M.; investigation, L.M., B.Ž. and T.S.; writing—original draft preparation, L.M.; writing—review and editing, B.Ž., T.S. and U.L.Š.; project administration, U.L.Š.; funding acquisition, U.L.Š. All authors have read and agreed to the published version of the manuscript.

Funding: This research was funded by the Slovenian Research Agency: research core funding No. P1-0134 and project No. L7-1848.

Conflicts of Interest: The authors declare no conflict of interest.

References

1. Matoh, L.; Žener, B.; Korošec, R.C.; Štangar, U.L. Photocatalytic Water Treatment. In *Nanotechnology in Eco-Efficient Construction*; Pacheco-Torgal, F., Vittoria Diamanti, M., Nazari, A., Goran Granqvist, C., Pruna, A., Amirkhanian, S., Eds.; Elsevier: Duxford, UK, 2019; Volume 4, pp. 675–702.
2. Ahmed, S.N.; Haider, W. Heterogeneous photocatalysis and its potential applications in water and wastewater treatment: A review. *Nanotechnology* **2018**, *29*, 342001–342031. [CrossRef]
3. Kanakaraju, D.; Glass, B.D.; Oelgemöller, M. Titanium dioxide photocatalysis for pharmaceutical wastewater treatment. *Environ. Chem. Lett.* **2014**, *12*, 27–47. [CrossRef]
4. Al-Mamun, M.R.; Kader, S.; Islam, M.S.; Khan, M.Z.H. Photocatalytic activity improvement and application of UV-tio$_2$ photocatalysis in textile wastewater treatment: A review. *J. Environ. Chem. Eng.* **2019**, *7*, 103248–103265. [CrossRef]
5. Crini, G.; Lichtfouse, E. Advantages and disadvantages of techniques used for wastewater treatment. *Environ. Chem. Lett.* **2019**, *17*, 145–155. [CrossRef]
6. Nakata, K.; Fujishima, A. TiO_2 photocatalysis: Design and applications. *J. Photochem. Photobiol. C Photochem. Rev.* **2012**, *13*, 169–189. [CrossRef]
7. Schneider, J.; Matsuoka, M.; Takeuchi, M.; Zhang, J.; Horiuchi, Y.; Anpo, M.; Bahnemann, D.W. Understanding TiO_2 photocatalysis: Mechanisms and materials. *Chem. Rev.* **2014**, *114*, 9919–9986. [CrossRef]
8. Hashimoto, K.; Irie, H.; Fujishima, A. TiO_2 Photocatalysis: A Historical Overview and Future Prospects. *Jpn. J. Appl. Phys. Part 1 Regul. Pap. Short Notes Rev. Pap.* **2005**, *44*, 8269–8285. [CrossRef]
9. Lee, S.Y.; Park, S.J. TiO2 photocatalyst for water treatment applications. *J. Ind. Eng. Chem.* **2013**, *19*, 1761–1769. [CrossRef]
10. Mahmoodi, N.M.; Arami, M.; Limaee, N.Y.; Tabrizi, N.S. Kinetics of heterogeneous photocatalytic degradation of reactive dyes in an immobilized TiO_2 photocatalytic reactor. *J. Colloid Interface Sci.* **2006**, *295*, 159–164. [CrossRef]
11. Visan, A.; Ruud Van Ommen, J.; Kreutzer, M.T.; Lammertink, R.G.H. Photocatalytic reactor design: Guidelines for kinetic investigation. *Ind. Eng. Chem. Res.* **2019**, *58*, 5349–5357. [CrossRef]
12. Shan, A.Y.; Ghazi, T.I.M.; Rashid, S.A. Immobilisation of titanium dioxide onto supporting materials in heterogeneous photocatalysis: A review. *Appl. Catal. A Gen.* **2010**, *389*, 1–8. [CrossRef]
13. Srikanth, B.; Goutham, R.; Badri Narayan, R.; Ramprasath, A.; Gopinath, K.P.; Sankaranarayanan, A.R. Recent advancements in supporting materials for immobilised photocatalytic applications in waste water treatment. *J. Environ. Manag.* **2017**, *200*, 60–78. [CrossRef] [PubMed]
14. Černigoj, U.; Štangar, U.L.; Trebše, P.; Ribič, P.R. Comparison of different characteristics of TiO_2 films and their photocatalytic properties. *Acta Chim. Slov.* **2006**, *53*, 29–35.
15. Nawi, M.A.; Zain, S.M. Enhancing the surface properties of the immobilized degussa P-25 TiO_2 for the efficient photocatalytic removal of methylene blue from aqueous solution. *Appl. Surf. Sci.* **2012**, *258*, 6148–6157. [CrossRef]
16. Bowering, N.; Walker, G.S.; Harrison, P.G. Photocatalytic decomposition and reduction reactions of nitric oxide over degussa P25. *Appl. Catal. B Environ.* **2006**, *62*, 208–216. [CrossRef]
17. Poulios, I.; Aetopoulou, I. Photocatalytic degradation of the textile dye reactive orange 16 in the presence of TiO_2 suspensions. *Environ. Technol. (UK)* **1999**, *20*, 479–487. [CrossRef]
18. Xiang, Q.; Yu, J. Photocatalytic activity of hierarchical flower-like TiO_2 superstructures with dominant {001} facets. *Chin. J. Catal.* **2011**, *32*, 525–531. [CrossRef]
19. Ling, Y.; Zhang, C.; Wu, J.; Xu, W.; Qi, Y.; He, P.; Zhao, L.; Guan, Y.; Zhang, Z.; Tian, Y. Enhanced photocatalytic activity of TiO_2 by micrometer-scale flower-like morphology for gaseous elemental mercury removal. *Catal. Commun.* **2018**, *116*, 91–95. [CrossRef]
20. Wu, Z.; Wu, Q.; Du, L.; Jiang, C.; Piao, L. Progress in the synthesis and applications of hierarchical flower-like TiO_2 nanostructures. *Particuology* **2014**, *15*, 61–70. [CrossRef]
21. Liu, M. Fabrication and photocatalytical properties of flower-like TiO_2 nanostructures. *Trans. Nonferrous Met. Soc. China* **2010**, *20*, 2299–2302. [CrossRef]
22. Song, H.; Chen, T.; Sun, Y.L.; Zhang, X.Q.; Jia, X.H. Controlled synthesis of porous flower-like TiO_2 nanostructure with enhanced photocatalytic activity. *Ceram. Int.* **2014**, *40*, 11015–11022. [CrossRef]
23. Liu, S.; Jaffrezic, N.; Guillard, C. Size effects in liquid-phase photo-oxidation of phenol using nanometer-sized TiO_2 catalysts. *Appl. Surf. Sci.* **2008**, *255*, 2704–2709. [CrossRef]